



Construction and validation of a prognostic nine-gene signature associated with radiosensitivity in head and neck squamous cell carcinoma

Congxian Lu^{a,b,1}, Qi Sun^{a,b,1}, Ying Guo^{a,b,1}, Xiao Han^{a,b}, Mingjun Zhang^{a,b}, Jiahui Liu^{a,b},
Yaqi Wang^{a,b}, Yakui Mou^{a,b}, Yumei Li^{a,b,*}, Xicheng Song^{a,b,*}

^a Department of Otorhinolaryngology, Head and Neck Surgery, Yantai Yuhuangding Hospital, Qingdao University, Yantai 264000, China

^b Shandong Provincial Clinical Research Center for Otorhinolaryngologic Diseases, China

ARTICLE INFO

Keywords:

Head and neck squamous cell carcinoma
Prognostic signature
Radiosensitivity
Immune cell infiltration

ABSTRACT

Background: Radiotherapy is an effective treatment for head and neck squamous cell carcinoma (HNSCC), however how to predict the prognosis is not clear.

Methods: Here we collected 262 radiosensitivity-associated genes, screened and constructed a prognostic nine-gene risk model through univariate COX, lasso regression, stepwise regression and multivariate COX analysis for transcriptome and clinical information of HNSCC patients obtained from the cancer genome atlas (TCGA) and gene expression omnibus (GEO) databases.

Results: The reliability and robustness of the risk model were verified by receiver operating characteristic (ROC) curves, risk maps, and Kaplan-Meier (KM) curves analysis. Differences in immune cell infiltration and immune-related pathway enrichment between high-risk and low-risk subgroups were determined by multiple immune infiltration analyses. Meanwhile, the mutation map and the responses to immunotherapy were also differentiated by the prognostic nine-gene signature associated with radiosensitivity. These nine genes expression in HNSCC was verified in the Human Protein Atlas (HPA) database. After that, these nine genes expression was verified to be related to radiation resistance through in-vitro cell experiments.

Conclusions: All results showed that the nine-gene signature associated with radiosensitivity is a potential prognostic indicator for HNSCC patients after radiotherapy and provides potential gene targets for enhancing the efficacy of radiotherapy.

Introduction

Head and neck squamous cell carcinoma (HNSCC) is the seventh most common cancer, accounting for 8.5 % new cancer cases and 4.8 % cancer-related deaths per year [1]. Radiotherapy is one of the main treatments for HNSCC [2], and the efficacy of radiotherapy is a

significant prognostic factor for clinical outcomes of HNSCC [3]. Due to the biological heterogeneity of HNSCC, responses to radiotherapy treatment varies widely between patients [4,5]. Responses to radiotherapy are affected by the radiobiological factors “6Rs”: DNA damage Repair, cell cycle Reassortment, Repopulation, Reoxygenation, cancer cell-intrinsic, Radiosensitivity, and antitumor immune Response [6,7].

Abbreviations: HNSCC, head and neck squamous cell carcinoma; RIS, radiosensitivity index; HRT, Hypofractionated radiation therapy; TME, tumor microenvironment; TCGA, the cancer genome atlas; GEO, gene expression omnibus; ROC, receiver operating characteristic; KM, Kaplan-Meier; Lasso, least absolute shrinkage and selection operator; TMB, tumor mutation burden; ICI, Immune checkpoint inhibitor; TIDE, Tumor Immune Dysfunction and Exclusion; IPS, Immunophenoscore; TCIA, The Cancer Immunome Atlas; GSEA, gene set enrichment analysis; IHC, immunohistochemistry; HPA, Human Protein Atlas; MRPL33, Mitochondrial Ribosomal Protein L33; MYOF, Myoferlin; VSIG4, V-Set and Immunoglobulin Domain Containing 4; RASGEF1B, RasGEF Domain Family Member 1B; TSPAN11, Tetraspanin 11; TCEA3, Transcription Elongation Factor A3; ING4, Inhibitor of Growth Family Member 4; TPPP3, Tubulin Polymerization Promoting Protein Family Member 3; HR, Hazard Ratio; NK, natural killer; CDKN2A, Cyclin Dependent Kinase Inhibitor 2A; TP53, Tumor Protein P53; TTN, Titin; FAT1, FAT Atypical Cadherin 1; JNK, c-Jun N-terminal kinase; DAMPs, Damage-Associated Molecular Patterns; STR, Short Tandem Repeat.

* Corresponding authors at: Department of Otorhinolaryngology, Head and Neck Surgery, Yantai Yuhuangding Hospital, Qingdao University, Yantai 264000, China.

E-mail addresses: myheart1263@163.com (Y. Li), drxchsong@163.com (X. Song).

¹ These authors contributed equally to the work.

<https://doi.org/10.1016/j.ctro.2023.100686>

Received 27 July 2023; Received in revised form 26 September 2023; Accepted 27 September 2023

Available online 2 October 2023

2405-6308/© 2023 The Authors. Published by Elsevier B.V. on behalf of European Society for Radiotherapy and Oncology. This is an open access article under the CC BY-NC-ND license (<http://creativecommons.org/licenses/by-nc-nd/4.0/>).

Differences in gene expression can affect cancer cell-intrinsic radiosensitivity and immune cell infiltration in the tumor microenvironment [8]. Predicting the efficacy of radiotherapy through gene expression is a challenge for the prognostic assessment of HNSCC. The gene-expression-based radiosensitivity index (RIS), which depends on the expression of 10 hub genes, was developed by Steven A. Eschrich from 48 cell lines including colorectal, renal, ovarian, prostate, lung, breast, and central nervous system cancers, as well as leukemias and melanomas [9,10]. The RIS was validated in multiple clinical cohorts including breast cancer [11,12], colon cancer [13], glioblastoma [14], pancreatic cancer [15], and endometrial cancer [16]. However, whether this model can recognize the immune cell infiltration and the anti-tumor immune responses remains unclear, especially in HNSCC.

Radiotherapy might enhance the priming of tumor-specific T cells to restore cancer sensitivity to immunotherapy [17]. Preclinical experiments have shown that cells irradiated with doses greater than 20 Gy for a short period of time exhibit the strongest effects, which suggested that Hypofractionated radiation therapy (HRT) might enhance the efficacy of radiation therapy [18,19]. HRT might derive irradiated tumor cells release Damage-Associated Molecular Patterns (DAMPs) to stimulate the differentiation and maturation of dendritic cells [20]. This is characterized by the upregulation of costimulatory molecules, resulting in improved T cell activation [18,19]. However, this effect was not demonstrated by clinical trials. Immune cells within the tumor microenvironment (TME) are associated with tumor radiosensitivity [21,22]. Evaluation of radiosensitivity associated genes may be used to assess optimal dosing and prognosis of radiotherapy in patients. These advances may help identify patients who are more likely to respond to RT.

In this study, we constructed and validated a prognostic signature containing nine radiosensitivity-associated genes for HNSCC patients through bioinformatics analysis and *in vitro* cell experiments.

Materials and methods

Collection of data

RNA-seq data, mutation data, and clinical information for 453 cases of head and neck squamous cell carcinoma (HNSCC) with patient survival time ≥ 30 days were obtained from The Cancer Genome Atlas (TCGA) database (<https://portal.gdc.ancer.gov/>). The RNA-seq data was re-annotated and transformed by $\log_2(x + 1)$ and standardized. The expression profile data and clinical information of 270 HNSCC cases with patient survival time ≥ 30 days were obtained from gene set GSE65858 from Gene Expression Omnibus (GEO; <https://www.ncbi.nlm.nih.gov/geo/>).

Acquisition of radiosensitivity-associated mRNAs

B.J.Thibodeau et al. used Affymetrix microarrays to compare gene expression between HNSCC patients who responded to radiotherapy and those who were radiotherapy non-responders, ultimately identifying 262 mRNAs that may indicate responsiveness to radiotherapy [23]. GO and KEGG enrichment analyses of these 262 radiosensitivity-associated mRNAs were carried out using the clusterProfiler R package [24].

Screening of radiosensitivity-associated gene signature

Univariate Cox analysis was performed to identify mRNAs associated with survival, those mRNAs with $P < 0.05$ were included into least absolute shrinkage and selection operator (Lasso) regression analysis [25]. Afterwards, stepwise regression was performed to further improve the predictive efficiency of the signatures [26].

Construction and evaluation of a radiosensitivity-associated prognostic gene signature

Multivariate Cox regression was used to establish a prognostic signature [27]. The risk score for each HNSCC patient sample was calculated as the expression value of each mRNA multiplied by the sum of their weights in the multivariable Cox regression. The median risk score was used to separate HNSCC patients into high and low-risk subgroups. Kaplan-Meier survival analysis was performed to compare survival differences between the high- and low-risk subgroups using the Survminer R package. Time-dependent Receiver operating characteristic (ROC) curve analysis was used to evaluate the predictive value of the prognostic signature using the time ROC R package.

Validation of the radiosensitivity-associated prognostic signature

To determine whether the risk score is an independent indicator of prognosis, univariate and multivariate Cox regression analysis were used to evaluate the prognostic relationship between age, gender, tumor size (T), lymph node metastasis (N), distant metastasis (M), clinical stage, and risk score. In addition, the accuracy of different clinicopathological factors and risk scores in predicting survival time were evaluated using the survival ROC R package. Finally, we construct a predictive model with the help of nomogram and use the calibration curves of 3- and 5-year to test the accuracy of the prediction model.

Estimation of mutation map and responses to immunotherapy

The maftools R package [28] was used to evaluate and quantify the mutation data and the tumor mutation burden (TMB) according to tumor-specific mutated genes in the high- and low-risk subgroups. Immune checkpoint inhibitor (ICI) responses were assessed by Tumor Immune Dysfunction and Exclusion (TIDE) score using the TIDE (<https://tide.dfci.harvard.edu/>) algorithm in the high- and low-risk subgroups. Immunophenoscore (IPS), calculated based on the gene expression in representative cell types, was used to determine the immunogenicity from four main cell types: effector cells, immunosuppressive cells, MHC molecules, and immunomodulators. The IPS of HNSCC patients were downloaded from The Cancer Immunome Atlas (TCIA) (<https://tcia.at/home>).

GSEA enrichment analysis and immune cells infiltration analysis

Functional enrichment scores were calculated by gene set enrichment analysis (GSEA) to identify the enriched GO biological processes and KEGG pathways in the high- and low-risk subgroups. CiberSort (<https://cibersort.stanford.edu/>) was used to assess the proportion of immune cells in the microenvironment of HNSCC samples. GSEA analysis between high-risk and low-risk subgroups was performed using the “maftools” R package on somatic mutation data downloaded from the TCGA database. In order to quantify the proportion of immune cells in HNSCC samples, we used CIBERSORT, MCPcounter, xCell, Quantiseq, and ssGSEA to compare the level of immune cell infiltration in high- and low-risk subgroups.

Validation of the protein expression levels of radiosensitivity-associated prognostic gene signature via the human protein atlas

To further verify the protein expression levels of the nine genes in colorectal cancer and normal tissues, immunohistochemistry (IHC) data were described from the Human Protein Atlas (HPA, <https://www.proteinatlas.org>), which can provide proteomics-based IHC results for multiple proteins in cancerous and normal tissues.

Construction of radioresistant cell lines

The hypopharyngeal carcinoma FaDu cell line was obtained from the Cell Bank of the Chinese Academy of Sciences (Shanghai, China). Cells were cultured in DMEM growth medium supplemented with 10 % fetal bovine serum (PAN, America), 100 U/ml penicillin and 100 mg/ml streptomycin at 37 °C in a humidified atmosphere of 5 % CO₂. The FaDu cell line was treated with X-ray irradiation ten times at 2 Gy, 2 Gy, 4 Gy, 4 Gy, 6 Gy, 6 Gy, 8 Gy, 8 Gy, 10 Gy, and 10 Gy in turn, for a cumulative total dose of 60 Gy using an American Varian Trilogy linear accelerator, with 6MV X-ray irradiation. The irradiation dose rate was 200 cGy/min, the distance of the source medium was 100 cm, and the culture flask was covered with 1.5 cm compensation. The final radioresistant FaDu cells were referred to as FaDuRR. Cell lines were authenticated by Short Tandem Repeat (STR) analysis as described in ANSI Standard (ANSI/ATCC ASN-0002–2011 Authentication of Human Cell Lines: Standardization of STR Profiling).

Colony formation assay

Both parental FaDu cells and FaDuRR cells were plated in 6-well plate with 1000 cells per well. And were irradiated with a single dose of 0, 4, 6 Gy, respectively. Cells were incubated for 14 days. Plates are filled with identical volumes of culture medium per well and are subsequently incubated in a humidified CO₂ incubator at physiological temperature for sufficient time to allow surviving cells to form colonies of ≥ 50 cells (a minimum of six population doublings). Finally, colonies are fixed with 4% paraformaldehyde (Biosharp, China) and stained with 0.1 % crystal violet (SparkJade, China). [29] Colonies of more than 50 cells and 100 cells were counted under microscope (ECHORVL-100-G) capture.

Quantitative real-time PCR verification

Total RNA was extracted using Trizol reagent from cancerous and paracancerous tissues of patients with HNSCC who had not received radiation therapy (n = 11), and from the FaDu and FaDuRR cells.

Total RNA was reverse transcribed into cDNA using HiScript III RT SuperMix for qPCR (+gDNA wiper Vazyme, China). Next, qRT-PCR was performed using ChamQ Universal SYBR qPCR Master Mix (Vazyme, China) in accordance with the manufacturer's instructions. Primer sequences are shown in Supplemental Table S1. The results were analyzed by the $2^{-\Delta\Delta Ct}$ method. Each experiment was repeated three times. Statistical significance between groups was evaluated by Student's t test, and $p < 0.05$ indicated a statistically significant difference.

Results

Construction and validation of radiosensitivity-associated prognostic gene signature

A total of 453 HNSCC patients' data (Supplementary Table S2) was obtained from TCGA database (flowchart detailing the analysis process is shown in Fig. 1). In brief, 262 radiosensitivity-associated genes were obtained from the B.J. Thibodeau et al. study [23] Functional enrichment analysis showed that the GO pathways most highly enriched among the 262 radiosensitivity-associated genes were the regulation of DNA replication, chromosome segregation, double-strand break repair via homologous recombination, and recombinational repair (Supplementary Fig. S1A). KEGG enrichment analysis showed that the associated genes are enriched in the p53 signaling pathway, homologous recombination, DNA replication, and chemical carcinogenesis-reactive oxygen species (Supplementary Fig. S1B).

Univariate Cox analysis of the 262 radiosensitivity-associated genes identified 30 mRNAs ($P < 0.05$) that were related to HNSCC prognosis (Fig. 2A, Supplementary Table S3). Among these, 22 mRNAs were further screened by Lasso regression (Fig. 2B, Supplementary Table S4). Next, forward-backward stepwise regression analysis was used to identify the most genes on HNSCC prognosis and narrow the signature down to 13 mRNAs (Supplementary Table S4). Finally, a nine gene radiosensitivity-associated prognostic signature was constructed by multivariate Cox analysis. This signature had significant characteristic value and contained candidate genes with the highest individual prognostic value (Fig. 2C, Supplementary Table S5). This signature contained

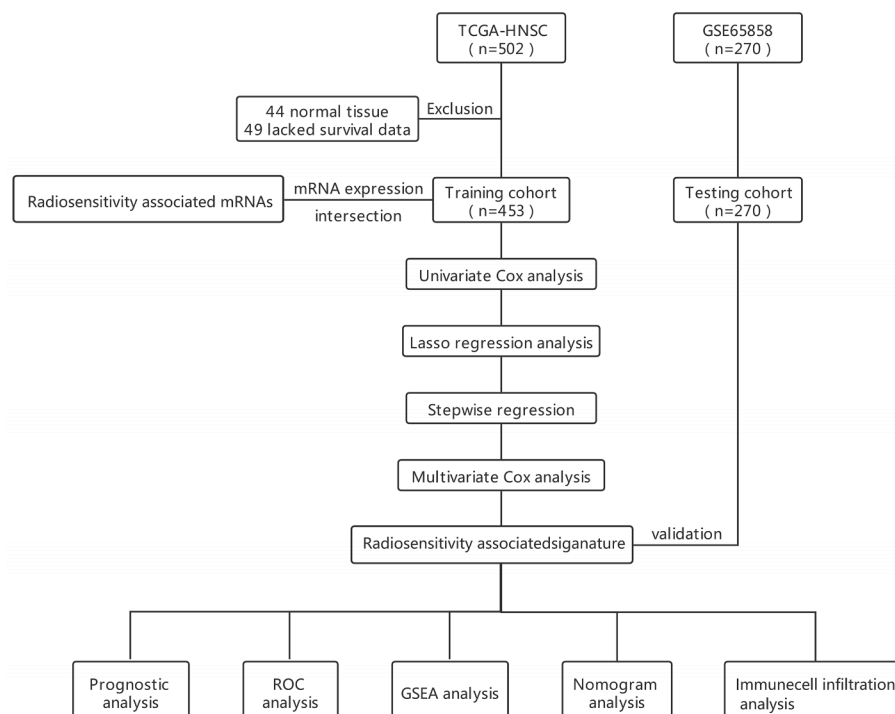


Fig. 1. Flowchart for the construction of the nine-gene radiosensitivity associated signature for prognosis.

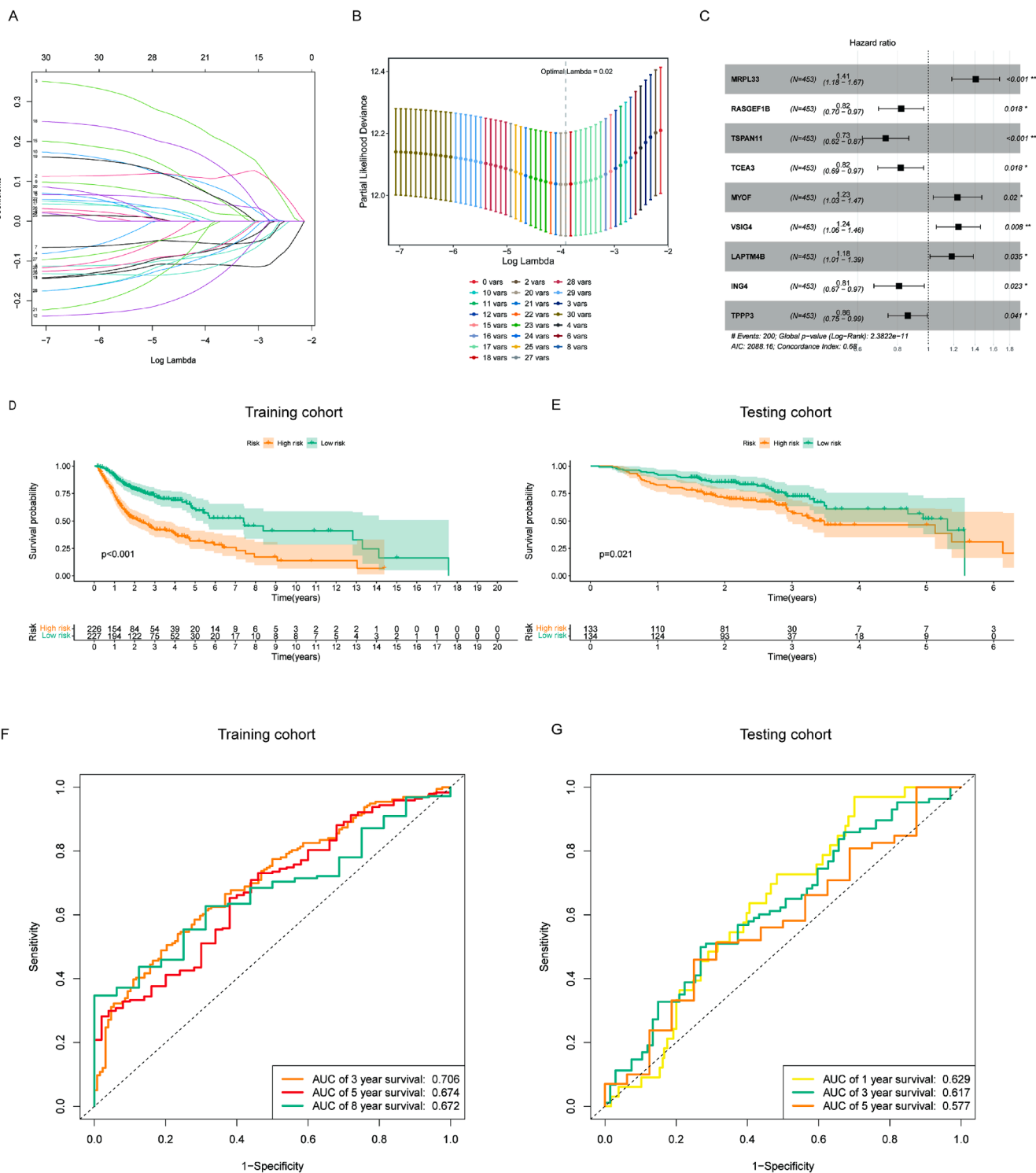


Fig. 2. The construction and verification of the radiosensitivity associated gene signature. (A) Lasso coefficient distribution of 30 mRNAs in the training cohort. (B) The coefficient profile was generated according to the logarithmic λ sequence. Selection of optimal parameter λ in the lasso model. (C) Lasso regression analysis screened forest maps of 9 candidate radiosensitivity mRNAs related to HNSCC survival in the construction of the prognostic signature. * $P < 0.05$, ** $P < 0.01$. (D-E) Verification of the radiosensitivity gene prognostic signature. The risk score level of the model-based classifier, Kaplan-Meier survival analysis was used to analyze the risk of death (overall survival) in (D) the training cohort and (E) the testing cohort. (F-G) Time-dependent receiver operating characteristic (ROC) analysis of the sensitivity and specificity of the survival for the nine-gene radiosensitivity-associated signature risk score in the (F) training cohorts and (G) testing cohorts.

4 mRNA risk factors: Mitochondrial Ribosomal Protein L33 (MRPL33), Myoferlin (MYOF), V-Set and Immunoglobulin Domain Containing 4 (VSIG4), and Lysosomal Protein Transmembrane 4 Beta (LAPTM4B) and 5 mRNA protective factors: RasGEF Domain Family Member 1B (RASGEF1B), Tetraspanin 11 (TSPAN11), Transcription Elongation Factor A3

(TCEA3), Inhibitor of Growth Family Member 4 (ING4), and Tubulin Polymerization Promoting Protein Family Member 3 (TPPP3), as identified by the cutoff of Hazard Ratio (HR) > 1 . The overall risk score for prognosis was calculated as $Risk\ score = \sum_i Expi(mRNA_i) * Coef(mRNA_i)$ where Expi is the expression value of each mRNA, and Coef is the

regression coefficient of the multivariate Cox analysis for the target mRNAs.

Following that, the HNSCC samples were divided into high-risk subgroups and low-risk subgroups based on the median risk score. The risk score and survival status of each HNSCC sample in the training cohort and the testing cohort were shown in a risk curve (Supplementary Fig. S2A and B) and scatter plot (Supplementary Fig. S2C and D). The risk coefficient and mortality in the high-risk subgroup was higher than those in the low-risk subgroup. RASGEF1B, TSPAN11, TCEA3, ING4, and TPPP3 were highly expressed in the low-risk subgroups, while MRPL33, MYOF, VSIG4 and LAPTM4B were highly expressed in the high-risk subgroups (Supplementary Fig. S2E). Kaplan-Meier analysis demonstrated that the overall survival (OS) of patients in the high-risk subgroup was worse than the low-risk subgroups in the training cohort (Fig. 2D, $P < 0.001$); this was verified in the testing cohort (Fig. 2E, $P = 0.021$). These results indicated that the risk score could effectively distinguish high-risk HNSCC patients from low-risk HNSCC patients. The AUC values analyzed by ROC for the 3-, 5-, and 10-year survival rates in the training cohort were 0.706, 0.674, and 0.672 respectively (Fig. 2F). The AUC values analyzed by ROC for 1-, 3-, and 5-year survival rates in the testing cohort were 0.629, 0.617, and 0.577, respectively (Fig. 2G). These results demonstrate that the nine-gene radiosensitivity-associated prognostic signature may be an effective prognostic marker for HNSCC.

The nine-gene radiosensitivity-associated prognostic signature is an independent predictive factor for HNSCC survival

Univariate and multivariate Cox regression analysis were used to explore whether the risk score of the nine-gene radiosensitivity-

associated prognostic signature was a prognostic factor independent of age, gender, pathological stage, and other clinicopathological factors. The risk scores and Hazard Ratios (HR) of univariate Cox regression analysis (Fig. 3A) and multivariate Cox regression analysis (Fig. 3B) were 2.099 with confidence interval 1.748–2.520 ($P < 0.001$), and 2.129 with confidence interval 1.765–2.568 ($P < 0.001$), respectively, suggesting that the risk score was an independent prognostic factor for HNSCC patients. In order to compare the sensitivity and specificity of risk score and clinicopathological factors on the prognosis of HNSCC patients, time-dependent ROC analysis was performed. The area under the ROC curve of the risk score was 0.662 (Fig. 3C), which was much higher than that of other clinicopathological factors. In addition, to improve the accuracy of prediction, a nomogram was integrated and constructed based on the statistically significant eigenvalues of the above multivariate Cox analysis results, including age, gender, tumor size (T), lymph node metastasis (N), distant metastasis (M), and risk score (Fig. 3D). The calibration curves of 3-year and 5-year survival probabilities predicted by the nomogram were in good agreement with the actual observed results (Fig. 3E). These results indicated that the risk score is a superior prognostic factor for HNSCC, and may be useful as an indicator to predict responses to radiotherapy in patients with head and neck tumors.

Differences in mutation status and responses to immunotherapy between high- and low-risk subgroups

Using the maftools R package [28], mutation data were analyzed and summarized based on the variant effect predictor. The top 30 driver genes with the highest alteration frequency in the high- and low-risk subgroups are shown in Fig. 4A and B. Tumor mutational burden

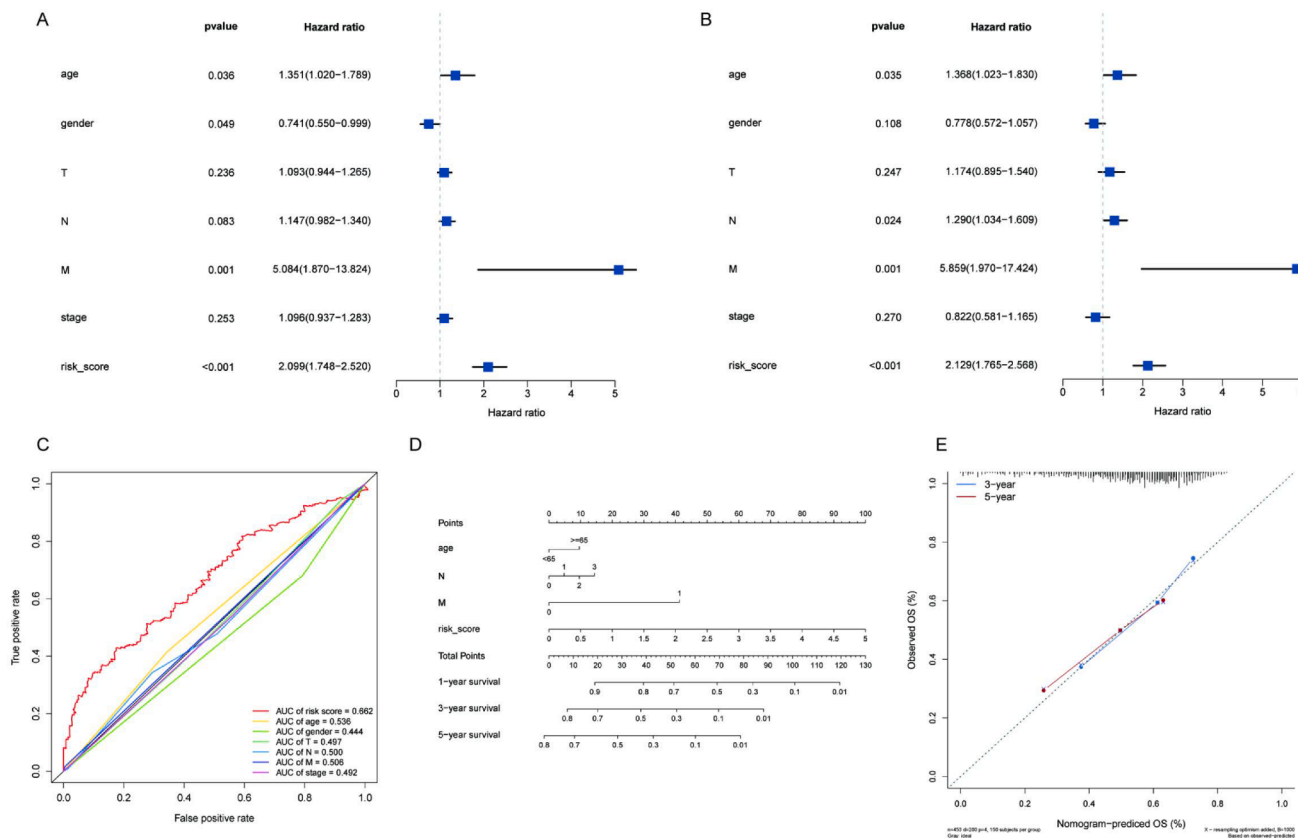


Fig. 3. Risk score analysis and nomogram construction to evaluate overall survival of HNSC patients. (A) Univariate Cox regression analysis of the model in the training cohort. (B) Multivariate Cox regression analysis of the risk score in the training cohort. (C) ROC analysis of the risk score and other clinicopathological factors for prediction of overall survival of HNSCC patients. (D) Nomogram for predicting the overall survival rate of HNSCC. (E) Nomogram calibration chart during 3-year and 5-year follow-up.

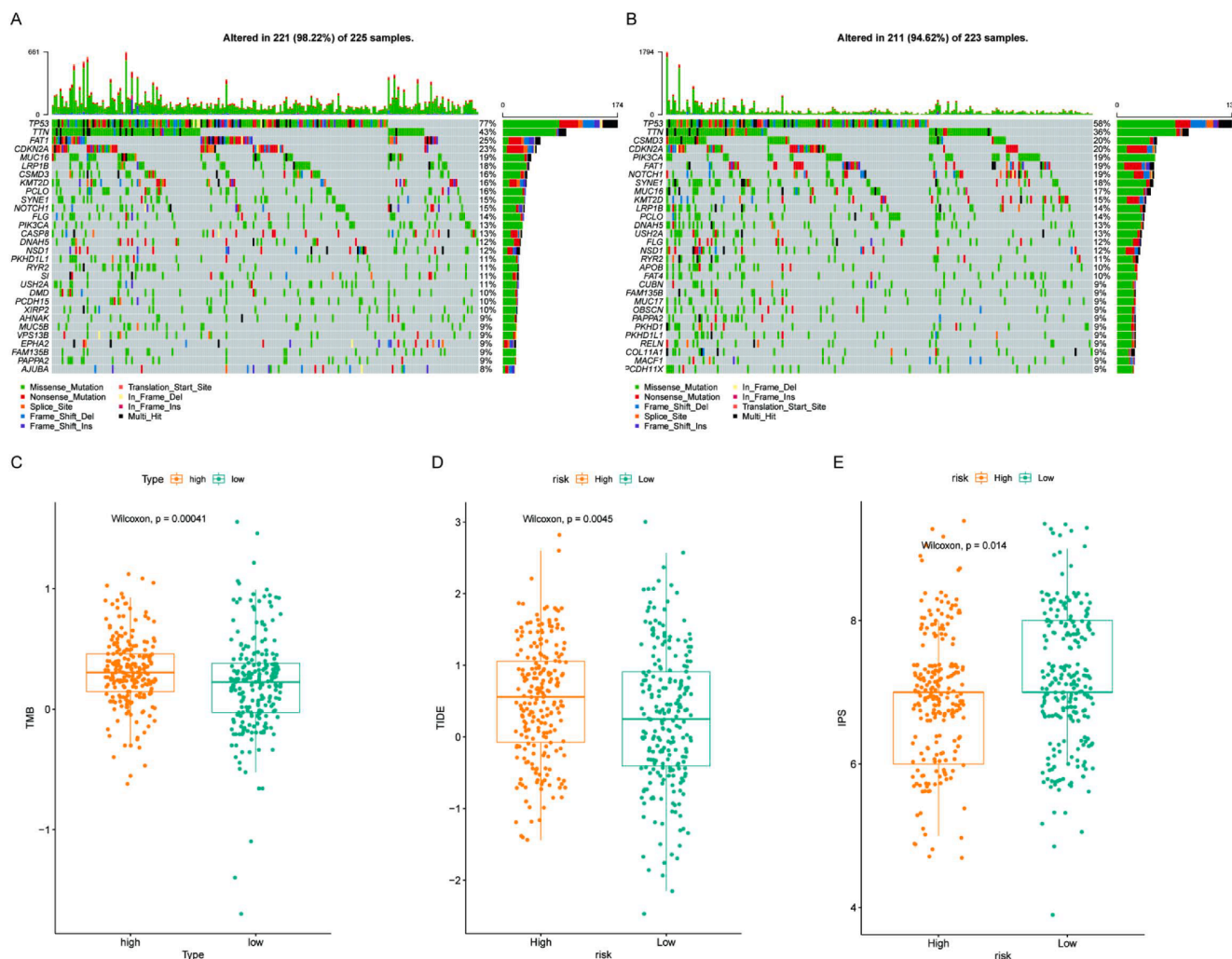


Fig. 4. Differences of mutation maps and responses to immunotherapy between high- and low-risk subgroups. (A-B) The mutations of the top 30 driver genes with the highest alteration frequency in the (A) high- and (B) low-risk subgroups. (C) Tumor mutational burden (TMB) in the high and low-risk subgroups (D) The Tumor Immune Dysfunction and Exclusion (TIDE) score in the high- and low-risk subgroups. (E) The Immunophenoscore (IPS) scores in the high- and low-risk subgroups.

(TMB) scores were calculated based on the TCGA somatic mutation data. The TMB scores in the high-risk subgroup were higher than the low-risk subgroup (Fig. 4C). Next, the responses to anti- Programmed Cell Death 1 (PD-1) and anti- Cytotoxic T-Lymphocyte Associated Protein 4 (CTLA4) immunotherapy in the high- and low-risk subgroups were assessed using the TIDE algorithm. The TIDE score was higher in the high-risk subgroup compared with the low-risk subgroup (Fig. 4D), suggesting that tumors in the low-risk group may be more sensitive to anti-PD-1 and anti-CTLA4 immunotherapy. In addition, the IPS scores were higher in the low-risk subgroup (Fig. 4E), suggesting that patients in the low-risk group might achieve a better response to immunotherapy. These results suggest that the nine-gene radiosensitivity-associated prognostic signature may also predict response to immunotherapy.

Gene enrichment analysis and immune infiltration analysis

In order to explore potential biological activities associated with the prognostic signature, functional enrichment analysis was performed for the differential expressed genes between the high- and low-risk subgroups. The high-risk subgroup was significantly enriched in the process of mitochondrial transport and in B cell and T cell receptor signaling pathways, P53 and JAK/STAT signaling pathways, and in pathways involved in regulating cell cycle and DNA replication. Immune-related

KEGG pathways associated with favorable prognosis were more significantly enriched in the low-risk subgroup than the high-risk subgroup, and included B cell and T cell receptor signaling pathway, CD4 positive or CD8 positive alpha beta T cell lineage commitment, mast cell activation in GO biological process, and the T cell receptor signaling (Fig. 5A, B and Supplementary Tables S6-S9). These findings suggest that higher levels of immune related gene expression and lower expression of DNA replication and cell cycle related genes could facilitate improved prognosis in the low-risk subgroups.

The immune cell infiltration in the tumor immune environment was analyzed by CiberSort, and compared between the high-risk and low-risk subgroups. Significant increases were identified in immune cell infiltration of plasma cells, CD4⁺ T cells, CD8⁺ T cells, T follicular helper cells, and mast cells in the low-risk subgroup vs. the high-risk subgroup, which may indicate more potent antitumor immune activity (Fig. 5C). We used CIBERSORT, MCPcounter, xCell, Quantiseq, and ssGSEA to calculate the level of immune cell infiltration in HNSCC samples. The numbers of immune cells with the strong anti-tumor activity, such as dendritic cells, natural killer (NK) cells, B cells, CD4 T cells, and CD8 T cells, were higher in the low-risk group than in the high-risk group (Fig. 5D-F). These findings suggest that among HNSCC samples, the low-risk group may have more active and robust anti-tumor immune properties, meaning this group may have a more favorable prognosis in terms of immunotherapy response and overall treatment effect.



Fig. 5. Computational analysis of immune cell infiltration in HNSCC tumors. (A-B) GSEA analysis. Results of functional enrichment of GSEA genes in different groups. (C) The differences in the estimation of infiltrating immune cells between the high-risk group and the low-risk group. * $P < 0.05$, ** $P < 0.01$, *** $P < 0.001$, **** $P < 0.0001$. (D) Heatmap depicting the frequency of tumor microenvironment infiltrating cells in two radioresistant-associated subtypes. The infiltration levels of different cell types in the low- and high-risk subgroups were analyzed using (E) CIBERSORT (F) MCPcounter, (G) Quantiseq, (H) ssGSEA, and (I) xCell.

Verification of the nine-gene radiosensitivity-associated prognostic signature in FaDu radiation resistant cells and in HNSCC tissue

Protein expression from the HPA database along with IHC results were shown in Fig. 6A. The proteins corresponding to the nine genes exhibited varying expression levels among different patients. TCEA3 and MYOF are moderately expressed in normal tissues, while MRPL33 is low-expressed and RASGEF1B is not detected. However, the proteins corresponding to these high-risk group mRNAs are not uniformly expressed in tumor tissues, and there are the above three situations. For example, MRPL33 has moderate or low expression in tumors, while TCEA3 has moderate or no expression. In the low-risk group, mRNAs TPP3 and VSIG4 were not detected in normal tissues, but there was low expression of ING4 and moderate expression of LAPTM4B. Likewise, the proteins corresponding to these genes were not uniformly expressed in tumor tissues, except for LAPTM4B, which was moderately expressed. It is worth noting that the expression of TSPAN11-related proteins is not collected in the HPA database, so graph A only shows the internal expression of eight-gene signature associated with radiosensitivity.

After that, we tested these nine gene expression change in radiotherapy resistance cells to check their function in radiotherapy resistance. As shown in Fig. 6B, more colonies survived in FaDuRR cells after irradiation. Counting of cell clusters with clones greater than 50 cells at OGY showed that FaDuRR was slightly higher than FaDu group (Fig. 6C), but there were more cell clusters greater than 100 cells in FaDuRR group (Fig. 6C). FaDuRR is more radioresistant than FaDu. QPCR results showed that the expression of RASGEF1B, TCEA3, ING4, TPP3, and TSPAN11 (Fig. 6D) decreased and MRPL33, MYOF, VSIG4, LAPTM4B (Fig. 6E) increased in FaDuRR cell line. However, the only significant expression differences between HNSCC tissue and paracancerous tissue were seen in TSPAN11, MYOF, and VSIG4 (Fig. 6F and G), indicating that differences in the expression of these genes may occur after radiotherapy treatment. Taken together, our findings demonstrate the important roles of these nine genes in HNSCC prognosis, especially in radiotherapy resistance, and provide important clues for in-depth understanding of their molecular mechanisms.

Discussion

Radiotherapy is the primary mode of treatment for HNSCC, however, many tumors exhibit radiotherapy resistance, which impairs the efficacy of radiotherapy [30]. In order to improve treatment for HNSCC it is important to improve the efficacy of radiotherapy and avoid radioresistance. In this study, we identified nine radiosensitivity-associated mRNAs by univariate Cox regression, Lasso regression, stepwise regression, and multivariate Cox regression to construct a nine-gene radiosensitivity associated prognostic signature. This signature may help provide more individualized risk-assessment for HNSCC treatment. The prognostic value of the nine-gene radiosensitivity-associated prognostic signature was confirmed and validated by rigorous computational techniques including Kaplan-Meier analysis, ROC analyses, and multivariate Cox regression. Our data suggested that this signature may provide prognostic indicators for HNSCC following radiotherapy, and might identify gene targets that could be used to enhance the efficacy of radiotherapy in HNSCC. It might potentially help guide the course of treatment and clinical decision making in patients at high risk of HNSCC.

Clinicopathological factors including age, gender, tumor size (T), lymph node metastasis (N), and distant metastasis (M) are related to the prognosis of HNSCC [31,32]. In our study, through univariate and multivariate Cox regression analysis, the clinicopathological factors age, N, M, and risk score were identified as independent clinical prognostic factors. ROC analysis and nomogram analysis showed that the risk score was an independent prognostic factor for HNSCC. These data suggest that the risk score is of great significance and could be used as a diagnostic indicator for the prognosis of radiotherapy.

Combination treatment of radiotherapy and immune checkpoint inhibitors (ICIs) is a promising strategy, due to effects including *in situ* tumor vaccination and radiation-induced cell death, which can initiate an immune stimulatory cascade. TMB predicts a favorable response to ICIs [33,34]. However, there is limited and conflicting evidence regarding the association between TMB and outcome after radiotherapy. In esophageal squamous cell carcinoma and cervical cancer, high TMB is associated with poorer OS [35,36], which is consistent with our study of mutation map analysis in high- and low-risk subgroups of HNSCC.

Prognostic gene expression signatures have been identified in HNSCC [37]. Several studies have demonstrated the clinical validity of multi-gene expression models of tumor radiosensitivity [9]. Tumors in high-risk subgroups have more genetic mutations and are less sensitive to radiotherapy. More frequent mutations in Tumor Protein P53 (TP53), Titin (TTN), Cyclin Dependent Kinase Inhibitor 2A (CDKN2A), and FAT Atypical Cadherin 1 (FAT1) were observed in the high-risk subgroup. Mutations in TTN and FAT1 are associated with cancer radiosensitivity and invasion in HNSCC [38,39]. This is consistent with our findings that mutation frequency in TTN and FAT1 was higher in the high-risk subgroup [40]. Mutations in TP53 and CDKN2A genes impact DNA repair that alter the radiosensitivity of tumors [41].

Radiation therapy causes DNA damage in tumors, leading to tumor cell death [42]. Genes associated with DNA damage repair can repair the DNA damage caused by radiotherapy, which can facilitate radiotherapy resistance of tumor cells [43]. In our study, we found that genes highly expressed in the high-risk subgroup were enriched in DNA damage repair, which may be a main factor contributing to high risk.

Differences in the distribution of immune cells in the tumor immune microenvironment, especially tumor-killing immune cells such as natural killer cells, CD8T cells, macrophages, and T follicular helper cells can lead to differences in disease prognosis [44]. GSEA enrichment analysis showed that there were significant differences in gene expression between high-risk and low-risk subgroups in DNA damage repair, immune cells, natural killer (NK) cell, and mast cell regulation, and a variety of immune responses. Immune cell infiltration analysis showed that immune cells beneficial to tumor killing are distributed more in tumors in the low-risk subgroup, indicating that the nine-gene radiosensitivity-associated prognostic signature may reflect the immune cell infiltration status of tumors and provide value to disease prognosis.

We found that the expression of RASGEF1B, TCEA3, ING4, TPP3, and TSPAN11 were reduced and the expression of MRPL33, MYOF, VSIG4 and LAPTM4B were increased in radiotherapy resistant HNSCC cells. Significant differences in expression levels of TSPAN11, MYOF, and VSIG4 were observed between HNSCC tissue and paracancerous adjacent tissue, suggesting that these genes may be related to HNSCC development. There were no significant expression differences of RASGEF1B, TCEA3, ING4, TPP3, MRPL33, and LAPTM4B between HNSCC tissue and paracancerous adjacent tissue, indicating that radiotherapy may change gene expression within the tumor, resulting in differential radiotherapy responses.

RASGEF1B is an immune-related enhancer RNA, is related to immune pathways and DNA damage regulation [45], and has prognostic value for bone metastasis of breast cancer [46]. Ectopic expression of TCEA3 inhibits cancer cell proliferation and induces tumor cell apoptosis by activating the c-Jun N-terminal kinase (JNK) pathway [47,48]. TCEA3 was highly downregulated in FaDuRR cells compared to FaDu cells, which may contribute to radiotherapy resistance. The membrane repair factors MYOF and LAPTM4B predict poor survival [49] and promote tumor growth [50,51] and metastasis in pancreatic cancer [52], breast cancer [53], colorectal cancer [54], and triple-negative breast cancer [55]. Expression of MYOF and LAPTM4B is related to drug resistance, and *de novo* chemoresistance to anthracyclines [56–58]. However, the functions of MYOF and LAPTM4B in HNSCC remain unclear. In our study, ectopic expression of MYOF and LAPTM4B contributed to radiotherapy resistance. This is supportive of previous reports, in which ectopic expression of MYOF and LAPTM4B

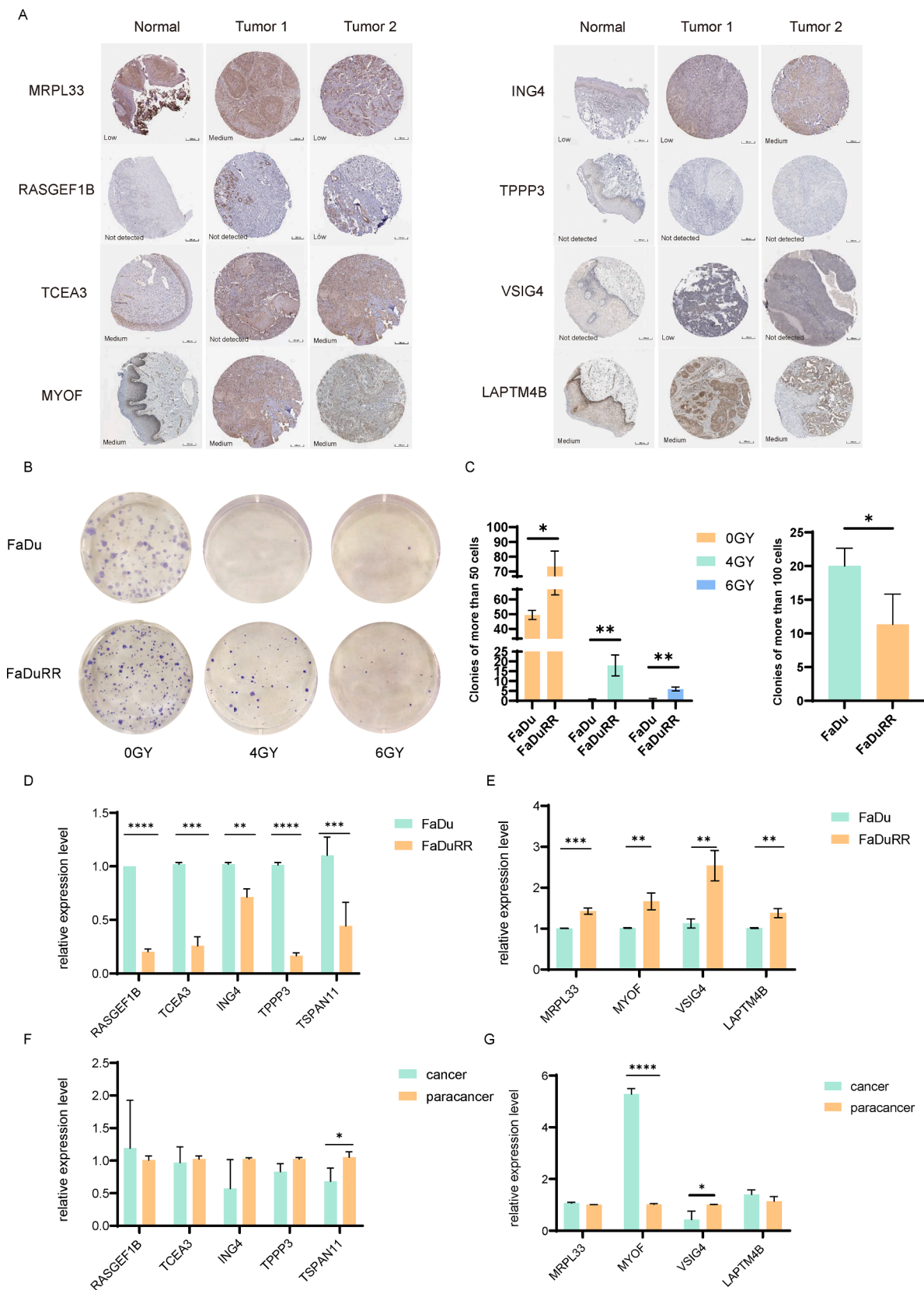


Fig. 6. Verification of expression of the nine-gene radiosensitivity-associated signature in HNSCC cell lines and tissues. (A) Protein expression of mRNAs corresponding to high and low risk groups in the HPA database. (B) Colony formation assay of FaDu and FaDuRR cell lines in 0GY, 4GY, 6GY group. (C) Colonies of FaDu and FaDuRR with more than 50 cells in 0GY, 4GY, 6GY group and more than 100 cells in 0GY group. (D-E) The expression of nine genes was verified in FaDu and FaDuRR cell lines. (F-G) Expression of nine genes in HNSCC tissue and in paracancerous tissue (n = 11).

promoted tumor progression and drug resistance.

VSIG4 protein is a B7 family related macrophage protein, which has the ability to inhibit T cell activation and has a potential role in cancer [59–61]. VSIG4 expression plays a critical role in the induction and maintenance of liver T- and Natural killer T (NKT)-cell tolerance [62], facilitates cancer development [63], and is associated with poor prognosis [64,65]. VSIG4 overexpression may inhibit tumor-killing immune responses and may be related to an increase in resting immune cells in the HNSCC microenvironment, thus contributing to radiotherapy resistance. Through bioinformatics analysis, TPPP3 and TSPAN11 were found to be associated with tumor immune infiltration of T cells, B cells, and bone marrow dendritic cells [66,67]. In our study, higher infiltration of B cells and CD8⁺ T cells was seen in the low-risk subgroup, which may be associated with lower TPPP3 and TSPAN11 expression in radioresistant cells. MRPL33 promotes chemosensitivity to epirubicin in gastric cancer [68], which is consistent with higher MRPL33 expression levels in radioresistant cells in our study.

Compared to other markers such as imaging, the analysis based on the expression levels of specific genes in tumor tissues or cells can take complex biological processes including intracellular signaling pathways and gene expression regulation into account. It can identify potential molecular targets, providing a basis for personalized therapy. Simon A. Keek et al. built a model for predicting overall survival in late-stage HNSCC patients using a multivariate Cox proportional hazards model incorporating 11 radiomic features extracted from diagnostic CT of primary tumors, along with clinical and biological variables, TNM8, and volume [69]. However, there are currently few relevant models for predicting radiotherapy sensitivity of HNSCC. Therefore, establishing a model, including monocular, protein, imaging characteristics, and clinical information, is necessary in the future.

In this study, we performed bioinformatics analysis to identify and validate a nine-gene radiosensitivity-associated prognostic signature for HNSCC. This signature provides a novel approach for stratification of HNSCC patients based on potential responsiveness to radiotherapy. However, there might be limitations related to data quality and patient heterogeneity. The incomplete clinical information, such as HPV status limited to include more clinical information in TCGA cohort. Additionally, it is crucial to consider the impact of ethnic diversity. Given that the TCGA database predominantly consists of information from patients of European and American descent, there is a notable gap in research pertaining to Asian populations. This may potentially constrain the applicability of our study findings across different ethnic groups. Therefore, when interpreting and generalizing the conclusions of our research, special attention should be paid to this aspect. Further validation and exploration in diverse populations, particularly among Asians, should be pursued whenever possible. Further clinical validation, including prospective studies or validation in independent cohorts, will be undertaken in the future through single-center or multi-center studies. Future studies should attempt to clarify the mechanisms of how the nine radiosensitivity associated genes regulate the tumor immune microenvironment and radiotherapy effects in HNSCC, and may provide new targets for the treatment of HNSCC.

Ethics approval and consent to participate

The study protocol was approved by the Ethics Committee of Yantai Yuhuangding Hospital, and the patients provided their informed consent for study participation. All methods were carried out in accordance with the Declaration of Helsinki.

Consent for publication

Not applicable.

Funding

This work was supported by the Taishan Scholars Project (No. ts20190991) and Science and Technology Innovation Development Plan of Yantai (No. 2022MSGY073).

Authors' contributions

XS and YL designed and directed the study. CL and QS organized the public data and wrote the manuscript. CL, QS, YG and XH performed experimental work. CL, JL, YW and MZ analyzed the data. XS, YL and YM revised the manuscript. All authors contributed to the article and approved the submitted version.

Declaration of Competing Interest

The authors declare that they have no known competing financial interests or personal relationships that could have appeared to influence the work reported in this paper.

Acknowledgements

This work was supported by the Taishan Scholars Project (No. ts20190991) and Science and Technology Innovation Development Plan of Yantai (No. 2022MSGY073).

Appendix A. Supplementary data Fig. 1: The functional enrichment analysis of (A) 453 HNSCC related genes and (B) 262 radiosensitivity related genes. Supplementary Fig. 2: Construction and evaluation of the 9-gene signature. (A–E) The 9-gene signature risk score analysis. The distribution of risk scores in (A) the training cohort and (B) the testing cohort. The distribution of the sample survival overview in (C) the training cohort and (D) the testing cohort. Green dots and red dots denote survival and death, respectively. (E) Heatmap of the expression profile distribution of the nine-gene signature among the low-risk group and high-risk group in the training cohort. The pink bar represents the low-risk subgroup and the blue bar indicates the high-risk subgroup.

Supplementary data to this article can be found online at <https://doi.org/10.1016/j.ctro.2023.100686>.

Reference

- [1] R.L. Siegel, K.D. Miller, H.E. Fuchs, A. Jemal, Cancer Statistics, 2021, CA: a cancer journal for clinicians, 71 (2021) 7–33.
- [2] Alterio D, Marvaso G, Ferrari A, Volpe S, Orecchia R, Jereczek-Fossa BA. Modern radiotherapy for head and neck cancer. *Semin Oncol* 2019;46:233–45.
- [3] D. Adelstein, M.L. Gillison, D.G. Pfister, S. Spencer, D. Adkins, D.M. Brizel, B. Burtness, P.M. Busse, J.J. Caudell, A.J. Cmelak, A.D. Colevas, D.W. Eisele, M. Fenton, R.L. Foote, J. Gilbert, R.I. Haddad, W.L. Hicks, Y.J. Hitchcock, A. Jimeno, D. Leizman, W.M. Lydiatt, E. Maghami, L.K. Mell, B.B. Mittal, H.A. Pinto, J.A. Ridge, J. Rocco, C.P. Rodriguez, J.P. Shah, R.S. Weber, M. Witek, F. Worden, S.S. Yom, W. Zhen, J.L. Burns, S.D. Darlow, NCCN Guidelines Insights: Head and Neck Cancers, Version 2.2017, Journal of the National Comprehensive Cancer Network : JNCCN, 15 (2017) 761–770.
- [4] Lawrence MS, Stojanov P, Polak P, Kryukov GV, Cibulskis K, Sivachenko A, et al. Mutational heterogeneity in cancer and the search for new cancer-associated genes. *Nature* 2013;499:214–8.
- [5] Razzouk S. Translational genomics and head and neck cancer: toward precision medicine. *Clin Genet* 2014;86:412–21.
- [6] Barker HE, Paget JT, Khan AA, Harrington KJ. The tumour microenvironment after radiotherapy: mechanisms of resistance and recurrence. *Nat Rev Cancer* 2015;15:409–25.
- [7] Sharabi AB, Lim M, DeWeese TL, Drake CG. Radiation and checkpoint blockade immunotherapy: radiosensitisation and potential mechanisms of synergy. *The Lancet Oncology* 2015;16:e498–509.
- [8] Scott JG, Berglund A, Schell MJ, Mihaylov I, Fulp WJ, Yue B, et al. A genome-based model for adjusting radiotherapy dose (GARD): a retrospective, cohort-based study. *The Lancet Oncology* 2017;18:202–11.

- [9] Eschrich SA, Pramana J, Zhang H, Zhao H, Boulware D, Lee JH, et al. A gene expression model of intrinsic tumor radiosensitivity: prediction of response and prognosis after chemoradiation. *Int J Radiat Oncol Biol Phys* 2009;75:489–96.
- [10] Eschrich S, Zhang H, Zhao H, Boulware D, Lee JH, Bloom G, et al. Systems biology modeling of the radiation sensitivity network: a biomarker discovery platform. *Int J Radiat Oncol Biol Phys* 2009;75:497–505.
- [11] Eschrich SA, Fulp WJ, Pawitan Y, Foekens JA, Smid M, Martens JW, et al. Validation of a radiosensitivity molecular signature in breast cancer, *Clinical cancer research : an official journal of the American Association for Cancer Res* 2012;18:5134–43.
- [12] Torres-Roca JF, Fulp WJ, Caudell JJ, Servant N, Bollet MA, van de Vijver M, et al. Integration of a radiosensitivity molecular signature into the assessment of local recurrence risk in breast cancer. *Int J Radiat Oncol Biol Phys* 2015;93:631–8.
- [13] Ahmed KA, Fulp WJ, Berglund AE, Hoffe SE, Dilling TJ, Eschrich SA, et al. Differences between colon cancer primaries and metastases using a molecular assay for tumor radiation sensitivity suggest implications for potential oligometastatic SBRT patient selection. *Int J Radiat Oncol Biol Phys* 2015;92:837–42.
- [14] Ahmed KA, Chinnaiyan P, Fulp WJ, Eschrich S, Torres-Roca JF, Caudell JJ. The radiosensitivity index predicts for overall survival in glioblastoma. *Oncotarget* 2015;6:34414–22.
- [15] Strom T, Hoffe SE, Fulp W, Frakes J, Coppola D, Springett GM, et al. Radiosensitivity index predicts for survival with adjuvant radiation in resectable pancreatic cancer. *Radiotherapy and Oncology : Journal of the European Society for Therapeutic Radiology and Oncology* 2015;117:159–64.
- [16] Mohammadi H, Prince A, Figura NB, Peacock JS, Fernandez DC, Montejo ME, et al. Using the radiosensitivity index (RSI) to predict pelvic failure in endometrial cancer treated with adjuvant radiation therapy. *Int J Radiat Oncol Biol Phys* 2020;106:496–502.
- [17] Dewan MZ, Galloway AE, Kawashima N, Dewyngaert JK, Babb JS, Formenti SC, et al. Fractionated but not single-dose radiotherapy induces an immune-mediated abscopal effect when combined with anti-CTLA-4 antibody. *Clin Cancer Res* 2009;15:5379–88.
- [18] Vanpouille-Box C, Formenti SC, Demaria S. Toward precision radiotherapy for use with immune checkpoint blockers. *Clin Cancer Res* 2018;24:259–65.
- [19] Krombach J, Hennel R, Brix N, Orth M, Schoetz U, Ernst A, et al. Priming anti-tumor immunity by radiotherapy: dying tumor cell-derived DAMPs trigger endothelial cell activation and recruitment of myeloid cells. *Oncoimmunology* 2019;8:e1523097.
- [20] Gupta A, Probst HC, Vuong V, Landshammer A, Muth S, Yagita H, et al. Radiotherapy promotes tumor-specific effector CD8+ T cells via dendritic cell activation. *J Immunol* 2012;189:558–66.
- [21] Shiao SL, Coussens LM. The tumor-immune microenvironment and response to radiation therapy. *J Mammary Gland Biol Neoplasia* 2010;15:411–21.
- [22] Yoshimura M, Itasaka S, Harada H, Hiraoka M. Microenvironment and radiation therapy. *Biomed Res Int* 2013;2013:685308.
- [23] Thibodeau BJ, Geddes TJ, Fortier LE, Ahmed S, Pruetz BL, Wobb J, et al. Gene Expression Characterization of HPV Positive Head and Neck Cancer to Predict Response to Chemoradiation. *Head Neck Pathol* 2015;9:345–53.
- [24] Wu T, Hu E, Xu S, Chen M, Guo P, Dai Z, et al. clusterProfiler 4.0: A universal enrichment tool for interpreting omics data. *Innovation (camb)* 2021;2:100141.
- [25] Sun Q, Li Y, Yang X, Wu X, Liu Z, Mou Y, et al. Identification and validation of 17-lncRNA related to regulatory T cell heterogeneity as a prognostic signature for head and neck squamous cell carcinoma. *Front Immunol* 2021;12:782216.
- [26] Schito L, Rey S, Xu P, Man S, Cruz-Muñoz W, Kerbel RS. Metronomic chemotherapy offsets HIF α induction upon maximum-tolerated dose in metastatic cancers. *EMBO Mol Med* 2020;12:e11416.
- [27] Guarnieri T, Filburn CR, Beard ES, Lakatta EG. Enhanced contractile response and protein kinase activation to threshold levels of beta-adrenergic stimulation in hyperthyroid rat heart. *J Clin Invest* 1980;65:861–8.
- [28] Mayakonda A, Lin DC, Assenov Y, Plass C, Koeffler HP. Maftools: efficient and comprehensive analysis of somatic variants in cancer. *Genome Res* 2018;28:1747–56.
- [29] Brix N, Samaga D, Belka C, Zitzelsberger H, Lauber K. Analysis of clonogenic growth in vitro. *Nat Protoc* 2021;16:4963–91.
- [30] Wang X, Hu C, Eisbruch A. Organ-sparing radiation therapy for head and neck cancer. *Nature reviews Clin Oncol* 2011;8:639–48.
- [31] Aupérin A. Epidemiology of head and neck cancers: an update. *Curr Opin Oncol* 2020;32:178–86.
- [32] Simard EP, Torre LA, Jemal A. International trends in head and neck cancer incidence rates: differences by country, sex and anatomic site. *Oral Oncol* 2014;50:387–403.
- [33] Sung H, Ferlay J, Siegel RL, Laversanne M, Soerjomataram I, Jemal A, et al. Global cancer statistics 2020: GLOBOCAN estimates of incidence and mortality worldwide for 36 cancers in 185 countries. *CA Cancer J Clin* 2021;71:209–49.
- [34] Marabelle A, Fakih M, Lopez J, Shah M, Shapira-Frommer R, Nakagawa K, et al. Association of tumour mutational burden with outcomes in patients with advanced solid tumours treated with pembrolizumab: prospective biomarker analysis of the multicohort, open-label, phase 2 KEYNOTE-158 study. *The Lancet Oncology* 2020;21:1353–65.
- [35] Ota N, Yoshimoto Y, Darwis NDM, Sato H, Ando K, Oike T, et al. High tumor mutational burden predicts worse prognosis for cervical cancer treated with radiotherapy. *Jpn J Radiol* 2021.
- [36] Yuan C, Xiang L, Cao K, Zhang J, Luo Y, Sun W, et al. The prognostic value of tumor mutational burden and immune cell infiltration in esophageal cancer patients with or without radiotherapy. *Aging* 2020;12:4603–16.
- [37] Chung CH, Parker JS, Karaca G, Wu J, Funkhouser WK, Moore D, et al. Molecular classification of head and neck squamous cell carcinomas using patterns of gene expression. *Cancer Cell* 2004;5:489–500.
- [38] Zuo Z, Ji S, He L, Zhang Y, Peng Z, Han J. LncRNA TTN-AS1/miR-134-5p/PAK3 axis regulates the radiosensitivity of human large intestine cancer cells through the P21 pathway and AKT/GSK-3 β / β -catenin pathway. *Cell Biol Int* 2020;44:2284–92.
- [39] Lin SC, Lin LH, Yu SY, Kao SY, Chang KW, Cheng HW, et al. FAT1 somatic mutations in head and neck carcinoma are associated with tumor progression and survival. *Carcinogenesis* 2018;39:1320–30.
- [40] Hutchinson MND, Mierzwa M, D'Silva NJ. Radiation resistance in head and neck squamous cell carcinoma: dire need for an appropriate sensitizer. *Oncogene* 2020;39:3638–49.
- [41] Wang M, Han J, Marcar L, Black J, Liu Q, Li X, et al. Radiation resistance in KRAS-mutated lung cancer is enabled by stem-like properties mediated by an osteopontin-EGFR pathway. *Cancer Res* 2017;77:2018–28.
- [42] Begg AC, Stewart FA, Vens C. Strategies to improve radiotherapy with targeted drugs. *Nat Rev Cancer* 2011;11:239–53.
- [43] Yang W, Wang L, Roehn G, Pearlstein RD, Ali-Osman F, Pan H, et al. Small ubiquitin-like modifier 1–3 conjugation [corrected] is activated in human astrocytic brain tumors and is required for glioblastoma cell survival. *Cancer Sci* 2013;104:70–7.
- [44] Tu B, Gao Y, Sun F, Shi M, Huang Y. Lipid metabolism regulation based on nanotechnology for enhancement of tumor immunity. *Front Pharmacol* 2022;13:840440.
- [45] England-Mason G, Merrill SM, Gladish N, Moore SR, Giesbrecht GF, Letourneau N, et al. Prenatal exposure to phthalates and peripheral blood and buccal epithelial DNA methylation in infants: an epigenome-wide association study. *Environ Int* 2022;163:107183.
- [46] Song Y, Pan Q, Xiao J, Li W, Ma H, Chen H, et al. Sialidase of *gliaeserella* parasitus augments inflammatory response via desialylation and abrogation of negative regulation of siglec-5. *Infect Immun* 2021;89.
- [47] Kazim N, Adhikari A, Oh TJ, Davie J. The transcription elongation factor TCEA3 induces apoptosis in rhabdomyosarcoma. *Cell Death Dis* 2020;11:67.
- [48] Cha Y, Kim DK, Hyun J, Kim SJ, Park KS. TCEA3 binds to TGF-beta receptor I and induces Smad-independent, JNK-dependent apoptosis in ovarian cancer cells. *Cell Signal* 2013;25:1245–51.
- [49] Blom T, Li S, Dichlberger A, Back N, Kim YA, Loizides-Mangold U, et al. LAPT4M4B facilitates late endosomal ceramide export to control cell death pathways. *Nat Chem Biol* 2015;11:799–806.
- [50] Li Y, Iglehart JD, Richardson AL, Wang ZC. The amplified cancer gene LAPT4M4B promotes tumor growth and tolerance to stress through the induction of autophagy. *Autophagy* 2012;8:273–4.
- [51] Li Y, Zhang Q, Tian R, Wang Q, Zhao JJ, Iglehart JD, et al. Lysosomal transmembrane protein LAPT4M4B promotes autophagy and tolerance to metabolic stress in cancer cells. *Cancer Res* 2011;71:7481–9.
- [52] Gupta S, Yano J, Mercier V, Htwe HH, Shin HR, Rademaker G, et al. Lysosomal retargeting of Myoferlin mitigates membrane stress to enable pancreatic cancer growth. *Nat Cell Biol* 2021;23:232–42.
- [53] Zhang T, Li J, He Y, Yang F, Hao Y, Jin W, et al. A small molecule targeting myoferlin exerts promising anti-tumor effects on breast cancer. *Nat Commun* 2018;9:3726.
- [54] He Y, Kan W, Li Y, Hao Y, Huang A, Gu H, et al. A potent and selective small molecule inhibitor of myoferlin attenuates colorectal cancer progression. *Clin Transl Med* 2021;11:e289.
- [55] Blomme A, Costanza B, de Tullio P, Thiry M, Van Simaey G, Boutry S, et al. Myoferlin regulates cellular lipid metabolism and promotes metastases in triple-negative breast cancer. *Oncogene* 2017;36:2116–30.
- [56] Harada K, Sakamoto N, Ukai S, Yamamoto Y, Pham QT, Taniyama D, et al. Establishment of oxaliplatin-resistant gastric cancer organoids: importance of myoferlin in the acquisition of oxaliplatin resistance. *Gastric Cancer* 2021;24:1264–77.
- [57] Meng Y, Wang L, Chen D, Chang Y, Zhang M, Xu JJ, et al. LAPT4M4B: an oncogene in various solid tumors and its functions. *Oncogene* 2016;35:6359–65.
- [58] Li Y, Zou L, Li Q, Haibe-Kains B, Tian R, Li Y, et al. Amplification of LAPT4M4B and YWHAZ contributes to chemotherapy resistance and recurrence of breast cancer. *Nat Med* 2010;16:214–8.
- [59] Kiyono K, Suzuki HI, Matsuyama H, Morishita Y, Komuro A, Kano MR, et al. Autophagy is activated by TGF-beta and potentiates TGF-beta-mediated growth inhibition in human hepatocellular carcinoma cells. *Cancer Res* 2009;69:8844–52.
- [60] Byun JM, Jeong DH, Choi IH, Lee DS, Kang MS, Jung KO, et al. The Significance of VSIG4 expression in ovarian cancer. *Int J Gynecol Cancer* 2017;27:872–8.
- [61] Vogt L, Schmitz N, Kurrer MO, Bauer M, Hinton HI, Behnke S, et al. VSIG4, a B7 family-related protein, is a negative regulator of T cell activation. *J Clin Invest* 2006;116:2817–26.
- [62] Jung K, Kang M, Park C, Hyun Choi Y, Jeon Y, Park SH, et al. Protective role of V-set and immunoglobulin domain-containing 4 expressed on kupffer cells during immune-mediated liver injury by inducing tolerance of liver T- and natural killer T-cells. *Hepatology* 2012;56:1838–48.
- [63] Liao Y, Guo S, Chen Y, Cao D, Xu H, Yang C, et al. VSIG4 expression on macrophages facilitates lung cancer development. *Lab Invest* 2014;94:706–15.
- [64] Kim SW, Roh J, Lee HS, Ryu MH, Park YS, Park CS. Expression of the immune checkpoint molecule V-set immunoglobulin domain-containing 4 is associated with poor prognosis in patients with advanced gastric cancer. *Gastric Cancer* 2021;24:327–40.

- [65] Xu T, Jiang Y, Yan Y, Wang H, Lu C, Xu H, et al. VSIG4 is highly expressed and correlated with poor prognosis of high-grade glioma patients. *Am J Transl Res* 2015;7:1172–80.
- [66] Liu J, Jiang C, Xu C, Wang D, Shen Y, Liu Y, et al. Identification and development of a novel invasion-related gene signature for prognosis prediction in colon adenocarcinoma. *Cancer Cell Int* 2021;21:101.
- [67] Yang Z, Li X, Li J, Su Q, Qiu Y, Zhang Z, et al. TPPP3 associated with prognosis and immune infiltrates in head and neck squamous carcinoma. *Biomed Res Int* 2020; 2020:3962146.
- [68] Li J, Feng D, Gao C, Zhang Y, Xu J, Wu M, et al. Isoforms S and L of MRPL33 from alternative splicing have isoform-specific roles in the chemoresponse to epirubicin in gastric cancer cells via the PI3K/AKT signaling pathway. *Int J Oncol* 2019;54: 1591–600.
- [69] Keek SA, Wesseling FWR, Woodruff HC, van Timmeren JE, Nauta IH, Hoffmann TK, et al. A prospectively validated prognostic model for patients with locally advanced squamous cell carcinoma of the head and neck based on radiomics of computed tomography images. *Cancers (basel)* 2021;13.